Compton Polarimetry

Douglas W. Storey
Supervisor: Dr. J. Martin
Honours Thesis

May 3, 2007

Abstract

The Qweak experiment, at Thomas Jefferson National Accelerator Facility, will test the Standard Model's predictions of the weak mixing angle, $\sin^2\theta_W$, through parity violating electron-proton scattering. Compton polarimetry will be used to measure the longitudinal polarization of the incident electron beam. In Compton polarimetry, the polarization is extracted from the Compton scattering asymmetry between laser light and electrons polarized parallel and anti-parallel. The asymmetry is measured by detecting the Compton scattered electrons. The electron detector will be a bulk semiconductor detector, fabricated from synthetic diamond. A GEANT simulation was used to model the polarimeter and to perform design studies related to the electron detector. Compton polarimetry theory, polarization extraction methods, and results of the design studies will be discussed.

Author: Douglas W. Storey

Thesis Supervisor: J. Martin
Thesis Committee: D. Vincent and S. Dannefaer

Contents

List of Figures

Chapter 1

The Qweak Experiment

1.1 The Standard Model

The Standard Model is the theory that describes interactions between the elementary particles. There are three different types of particles; leptons, quarks and mediators. They each have fundamental properties associated with them such as charge, mass and spin. The particles interact through gravity, electromagnetism, and the strong and weak forces. The Standard Model includes descriptions of three of the four fundamental forces but does not include a description of gravity.

Since its introduction in the 1970's, the Standard Model has been very successful. It predicted the existence of certain particles before they were ever observed, it predicts accurate values to some quantities included in the model such as the masses of the W and Z bosons, and it has agreed with all experimental tests.

Experimental tests are very important in the formulation of the Standard Model. It includes many free parameters that cannot be determined within the framework of the theory itself and must be determined experimentally. Tests are also important to guide transformations in the theory or to rule out possible expansions.

The electromagnetic and weak forces have been unified into a single force, the electroweak interaction, where the electromagnetic and weak interactions are different manifestations of the same basic interaction. Electromagnetic interactions are mediated by massless photons, and the weak force by the extremely massive W and Z bosons.

In this theory, the Glashow-Weinberg-Salam theory [1], the observable photons and Z^0 bosons are formed from linear combinations of the neutral W and B^0 bosons. The W and B bosons mix to produce the photon, γ, and the Z^0 bosons according to the so called weak mixing angle, θ_W, via:

$$A = B^0\cos\theta_W + W^0\sin\theta_W \tag{1.1}$$
$$Z = -B^0\cos\theta_W + W^0\sin\theta_W \tag{1.2}$$

Where A and Z refer to the photon and Z^0 boson fields.

The weak mixing angle also gives relationships between the weak coupling constants, g_W and g_Z, to the electromagnetic coupling constant, g_e,

$$g_W = \frac{g_e}{\sin\theta_W} \text{ and } g_Z = \frac{g_e}{\sin\theta_W\cos\theta_W} \ . \tag{1.3}$$

The coupling constants, g_e, g_W, and g_Z, determine the strength of the interactions.

The weak mixing angle is not a constant but varies as a function of the energy at which it is measured, Q. This is due to the fact that the effective coupling depends on the distance to the source. For example, in quantum electrodynamics, virtual electron-positron pairs, such as in the Feynman diagram in Figure 1.1, screen the target particle's charge and reduces the coupling. This is called *vacuum polarization*. Due to these higher order corrections the weak charge and hence $\sin^2\theta_W$ vary with energy.

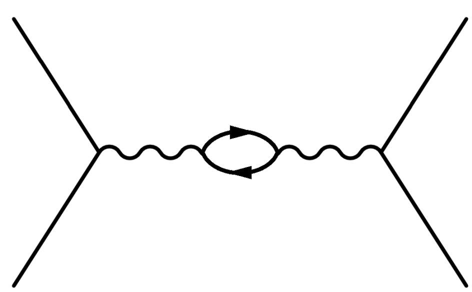

Figure 1.1: **Vacuum polarization in quantum electrodynamics**

The Standard Model predicts how $\sin^2\theta_W$ varies with Q, where Q^2 is the negative four-momentum transfer squared. This is shown by the blue line on the plot in Figure 1.2. The width of the line represents the uncertainty in the Standard Model calculations. Also shown on Figure 1.2 are past and future experiments measuring the value of $\sin^2\theta_W$ at various energies. The black points on the plot represent the past measurements, and the red points are proposed future experiments with their expected uncertainties. The future experiments are placed at the proposed Q and an arbitrarily chosen vertical position.

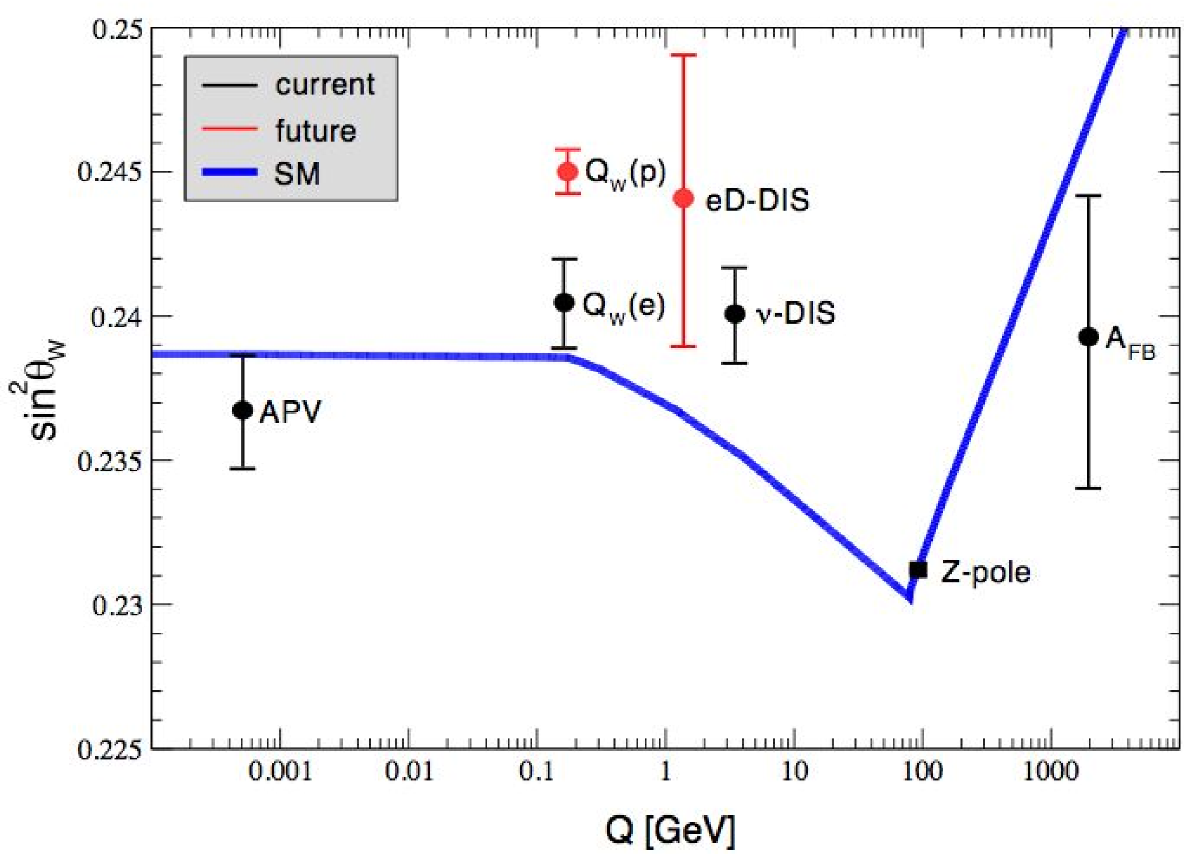

Figure 1.2: **The running of $\sin^2\theta_W$.** The line represents the prediction of $\sin^2\theta_W$ by the Standard Model. [7]

The most accurate measurement at high energy was performed at the Z-pole [3]. However, to test the running of $\sin^2\theta_W$, this precise measurement must be compared with other low-energy experiments. There have been several measurements done at lower energy through Atomic Parity Violation (APV) [4], the measurement of the weak charge of the electron ($Q_W(e)$) [5], and neutrino scattering (ν-DIS) [6]. The first two experiments, APV and $Q_W(e)$, were found to agree with the theory whereas the ν-DIS measurement lies three standard deviations off the expected result. The Qweak experiment ($Q_W(p)$) is also included on Figure 1.2, at the proposed beam energy, to show the proposed error bar. The Qweak measurement will be the most precise measurement of $\sin^2\theta_W$ below the Z-pole.

1.2 Qweak

The Qweak experiment will test the Standard Model's predictions of the running of $\sin^2\theta_W$ to low energy. The experiment will take place at the Thomas Jefferson National Accelerator Facility (JLab) in Newport News, Virginia and will use electron-proton scattering to make the most precise measurement of the weak force at low energy [2]. A deviation of $\sin^2\theta_W$ from the expected theoretical value would signify physics beyond the Standard Model. Examples of such extensions are supersymmetry, extra neutral gauge interactions beyond the photon and Z boson, and leptoquarks. Agreement would place new constraints on such expansions of the Standard Model.

Through the precise measurement of the weak charge of the proton, $Q_W(p)$, $\sin^2\theta_W$ can be extracted through the relation, $Q_W(p) = 1 - 4\sin^2\theta_W$, to lowest order. $Q_W(p)$ can be experimentally determined by measuring the asymmetry between cross-sections for positive and negatively polarized electrons in electron-proton scattering.

To lowest order, electron-proton scattering occurs through the exchange of either a photon or a Z^0 boson as shown in Figure 1.3. The asymmetry in the cross-section is a result of parity violation arising from the interference of electromagnetic and weak amplitudes.

At low energy and small (forward) scattering angles, the parity violating electron-proton scattering asymmetry is given by

$$A_{ep} = \frac{\sigma^+ - \sigma^-}{\sigma^+ - \sigma^-} = -\frac{G_F Q^2}{4\sqrt{2}\pi\alpha}\left(Q_W(p) - Q^2 B(Q^2)\right) \tag{1.4}$$

where $\sigma^\pm$ are the cross sections for positive or negative incident electron helicities, G_F is the Fermi constant, Q^2 is the negative four-momentum transfer squared, and $B(Q^2)$ is a

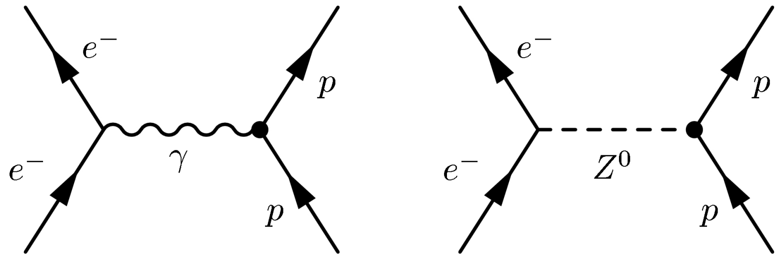

Figure 1.3: **Electron-proton scattering.** First order Feynman diagrams for electron proton scattering through the exchange of a photon, left, and a Z^0 boson, right.

contribution from electromagnetic and weak form factors.

A schematic diagram of the Qweak experiment is shown in Figure 1.4. The longitudinally polarized beam of electrons, with energy $E = 1.165\,\mathrm{GeV}$ and at a current of $180\,\mu\mathrm{A}$, impinges on a liquid hydrogen target. Electrons scattered at forward angles will be selected by several collimators and focused by a toroidal magnet onto the quartz Čerenkov detectors.

The asymmetry will be measured to a combined statistical and systematic error of 2.2% which will result in an extraction of $Q_W(p)$ to an accuracy of 4.1%. The systematic breakdown is shown in Table 1.1. As can be seen from the table, the dominant experimental systematic uncertainty arises from the uncertainties due to the electron beam polarization. To obtain the required accuracy in $Q_W(p)$, the polarization of the beam must be known to an relative accuracy of 1%. This can accomplished through Compton Polarimetry.

Source	$\delta A_{ep}/A_{ep}$	$\delta Q_W(p)/Q_W(p)$
Counting statistics	1.8 %	2.9 %
Hadronic structure	-	1.9 %
Beam polarimetry	**1.0 %**	**1.6 %**
Absolute Q^2	0.5 %	1.1 %
Backgrounds	0.5 %	0.8 %
Hel.-corr. beam props.	0.5 %	0.8 %
Total	2.2 %	4.1 %

Table 1.1: **Contributions to the error in A_{ep} and $Q_W(p)$ for Qweak.**

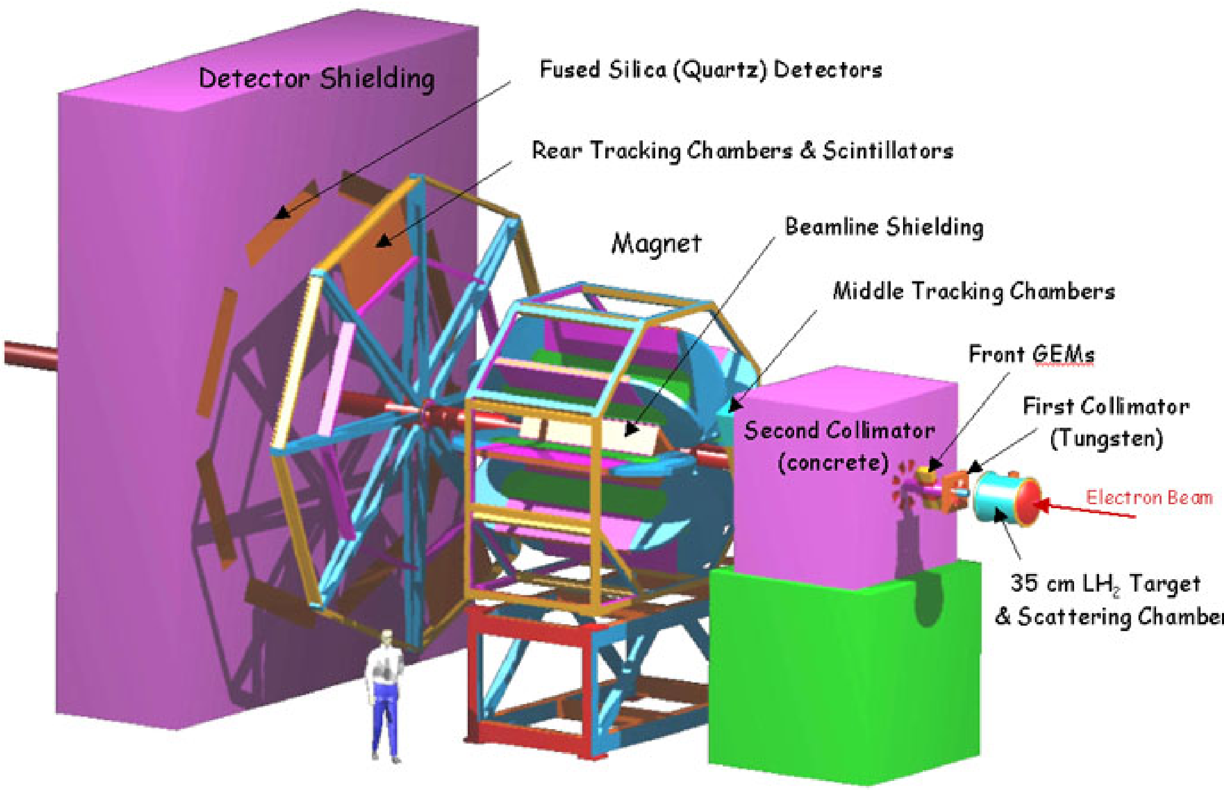

Figure 1.4: **Schematic of the Qweak experimental setup.** [7]

Chapter 2

Compton Polarimetry

Compton scattering is the scattering of a photon off an electron. The cross section for this interaction depends on the relative alignment of the spins of the two interacting particles. This property is the basis for Compton polarimetry.

2.1 Kinematics

In electron scattering experiments, the electron beam is made up of individual electrons, moving along the z-axis with an energy E, as shown in Figure 2.1. The four-momentum of one of these electrons can be denoted by the 4-vector $p = (E;\, 0,\, 0,\, p)$. In Compton scattering, an incoming photon, denoted by $k = (k;\, k\sin\alpha,\, 0,\, -k\cos\alpha)$, where α is the angle of the incoming photon with respect to the beam axis, hits the electron. The photon source is a high-power green laser.

The electron imparts some of its energy to the photon, and is deflected from the main beam line by an angle θ_e. The *recoil electron* thus has 4-momentum $p' = (E';\, p'\sin\theta_e,\, 0,\, p'\cos\theta_e)$. The photon scatters at an angle θ_γ, and $k' = (k';\, k'\sin\theta_\gamma,\, 0,\, -k'\cos\theta_\gamma)$.

Applying conservation of 4-momentum, i.e. $p^\mu + k^\mu = p'^\mu + k'^\mu$, the energy of the scattered photon can be found in terms of the incident photon and electron parameters as

$$k' = k\frac{E + p\cos\alpha}{E + k - p\cos\theta_\gamma + k\cos(\theta_\gamma - \alpha)}, \tag{2.1}$$

and the energy of the recoil electron is

$$E' = E + k - k'\ . \tag{2.2}$$

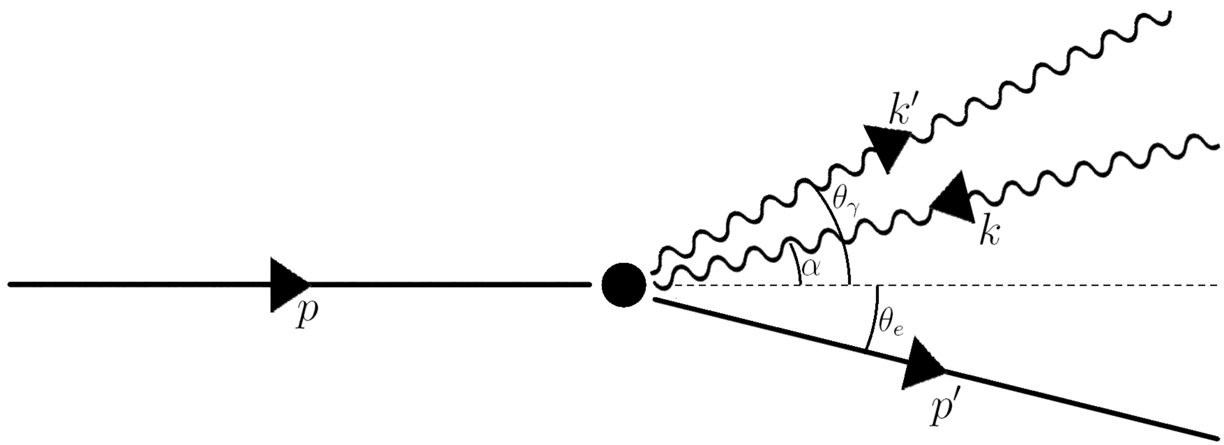

Figure 2.1: **Compton scattering of free electrons**

In most cases it is arranged experimentally such that $\alpha \cong 0$. This is done to maximize the intersecting volume of the electron and photon beams and hence increase the likelihood of Compton scattering. Therefore we shall analyze the case where $\alpha = 0$ more explicitly.

Defining the photon energy relative to the maximum, $\rho = k'/k$, and using $\gamma = E/m_e$, for small photon scattering angles, (2.1) becomes

$$\rho = k'/k \cong \frac{4\gamma^2}{1 + \frac{4k\gamma}{m_e} + \theta_\gamma^2\gamma^2} = \frac{4a\gamma^2}{1 + a\theta_\gamma^2\gamma^2} \ , \tag{2.3}$$

where a is the kinematical parameter,

$$a = \frac{1}{1 + \frac{4k\gamma}{m_e}} \ . \tag{2.4}$$

A photon scattering angle of $\theta_\gamma = 0$, corresponds to the maximum scattered photon energy, $k' = k'_{max}$, i.e. the Compton edge, and minimum recoil electron energy. Thus at the Compton edge

$$k'_{max} = \frac{4akE^2}{m_e^2} \quad \text{and} \quad E_{min} = E + k - \frac{4akE^2}{m_e^2} \ . \tag{2.5}$$

The kinematical parameters for Qweak are summarized in Table 2.1.

Parameter	Value
Beam energy, E	1.165 GeV
Laser wavelength, λ	514 nm
Laser energy, k	2.412 eV
Kinematical parameter, a	0.9587
Compton edge, k'_{max}	48.08 MeV
Compton edge, E'_{min}	1.117 GeV
Maximum electron scattering angle $\theta_{e,max}$	9.44 μrad

Table 2.1: **Qweak kinematical parameters.**

2.2 Compton Cross Section

The Compton scattering cross section is a measure of the likelihood of an incident photon interacting with an electron. The cross section can be calculated in Quantum Electrodynamics. The two leading-order Feynman diagrams for Compton Scattering are shown in Figure 2.2.

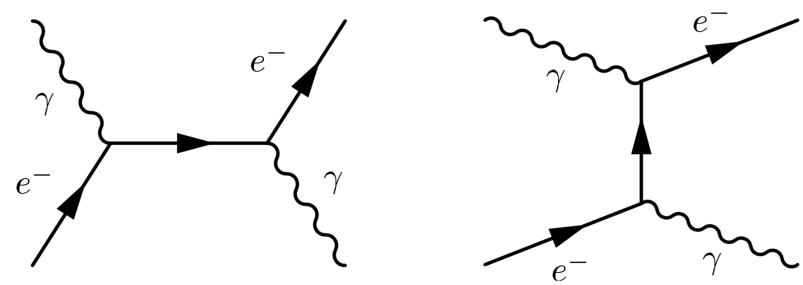

Figure 2.2: **Feynman diagrams for Compton Scattering**

For a laser crossing angle of $\alpha = 0$, the differential unpolarized cross section, with respect to ρ, the scattered photons energy relative to the maximum, is [8]

$$\frac{d\sigma}{d\rho} = 2\pi r_0^2 a \left[\frac{\rho^2(1-a)^2}{1-\rho(1-a)} + 1 + \left(\frac{1-\rho(1+a)}{1-\rho(1-a)} \right)^2 \right] \tag{2.6}$$

where r_0 is the classical radius of the electron.

The unpolarized cross section varies smoothly as function of energy, as shown in Figure 2.3. The Compton edge, $\rho_{max} = 1$, is the kinematical limit on scattered photon energies. All of the scattered photons have an energy less than this maximum energy.

The total differential Compton scattering cross section, $\frac{d\sigma}{d\rho}^{\pm}$, is the sum of the unpolarized and polarized cross sections, $\frac{d\sigma}{d\rho}$ and $\frac{d\sigma}{d\rho}_p$,

$$\frac{d\sigma}{d\rho}^{\pm} = \frac{d\sigma}{d\rho} \pm \frac{d\sigma}{d\rho}_p \quad . \tag{2.7}$$

where $\frac{d\sigma}{d\rho}^{+}$ is the cross section for the electron and photon polarized parallel, and $\frac{d\sigma}{d\rho}^{-}$ for the polarizations opposite each other.

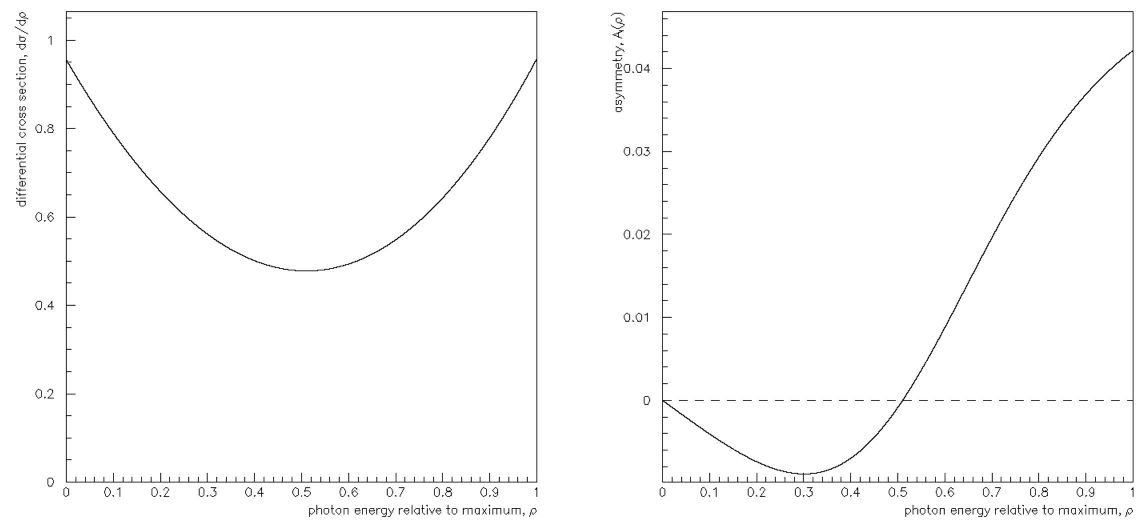

Figure 2.3: **Differential unpolarized Compton cross section, and Compton asymmetry for the Qweak kinematics.** Electron beam energy of $E = 1.165\,\mathrm{GeV}$ and laser energy of $k = 2.412\,\mathrm{eV}$

2.3 Compton Asymmetry

The theoretical longitudinal asymmetry, A_ℓ, for the Compton scattering of electrons and photons with spins parallel, σ^+, and spins anti-parallel, σ^-, is given by

$$A_\ell = \frac{\sigma^+ - \sigma^-}{\sigma^+ + \sigma^-} \ , \tag{2.8}$$

where σ is used here as shorthand notation for the differential cross section, $\frac{d\sigma}{d\rho}$. The asymmetry is related to the unpolarized differential cross section (2.7) by [8]

$$A_\ell = \frac{2\pi r_0^2 a}{\frac{d\sigma}{d\rho}} \left(1 - \rho(1+a)\right) \left(1 - \frac{1}{\left(1 - \rho(1-a)\right)^2}\right) \quad . \tag{2.9}$$

Since the electron beam is never 100% linearly polarized and the laser 100% circularly polarized, the experimentally measured asymmetry, A_{exp}, is related to the theoretical asymmetry through the polarizations of the electron beam, P_e, and the scattering photons in the laser beam, P_γ, by

$$A_{exp} = \frac{n^+ - n^-}{n^+ + n^-} = P_e P_\gamma A_\ell \ , \tag{2.10}$$

where n^+ is the number of Compton scattering events with electron and photon spins parallel, and n^- with the spins anti-parallel.

A plot of the Compton asymmetry for the Qweak kinematics, as a function of the scattered photon energy, is given in Figure 2.3. The asymmetry approaches zero when the scattered photon energy is zero. It is negative for low scattering energies and crosses through zero, the *asymmetry zero*, when the scattered energy is approximately half of the maximum energy, ρ_0. The asymmetry is maximum at the Compton edge, $\rho_{max} = 1$.

For the proposed laser and beam energies, the maximum asymmetry is $A_{max} = 0.0421$, and the zero-crossing is found at $\rho_0 = 0.512$.

The longitudinal polarization of the electron beam, P_e, can be determined from the experimental Compton asymmetry trivially from equation (2.10):

$$P_e = \frac{A_{exp}}{P_\gamma A_\ell} \ , \tag{2.11}$$

where A_{exp} is the asymmetry measured experimentally using electron or photon detectors, P_γ is the polarization of the laser beam, and A_ℓ is the theoretical asymmetry, equation (2.9).

To measure the polarization of the electron beam, the Compton asymmetry must be mapped out as a function of the scattered photon energy. This is achieved by measuring the number of Compton events at each scattered energy by detecting either the scattered photons or the recoil electrons, or, as will be done in Qweak, both.

2.4 Magnetic Chicane

To measure the polarization of the electron beam, the recoil electrons must be detected without disrupting the unscattered electrons in the main beam line. The high energy electrons are deflected away from the main beam line by a tiny angle in Compton scattering. It would take over 500 m to get a deflection of only 5 mm from the beam line with the proposed laser and beam energies, which is not practical.

A *magnetic chicane* can be used to deflect the electrons from the main beam line in much less space than by Compton scattering alone. The magnetic chicane deflects the electrons according to their momentum; lower momentum electrons are deflected by a larger amount than higher momentum electrons. This is called *momentum analyzing*, as the deflection of the electron is a function of the electron's momentum.

When an electron, with charge e and moving at velocity $\vec{v}$, travels through a magnetic field $\vec{B}$, it experiences a force, $\vec{F}_{mag} = e(\vec{v} \times \vec{B})$, which causes the electron to move in a circular path, with radius

$$R = \frac{\gamma m_e v}{eB} = \frac{p}{eB} \tag{2.12}$$

where $\gamma = \frac{1}{(1-\beta^2)^{1/2}}$, $\beta = \frac{v}{c}$, m_e is the mass of the electron, and p is the relativistic momentum of electron, $p = \gamma m_e v$.

Electrons with a lower momentum are deflected more in a magnetic field than electrons with higher energy. The magnetic chicane uses this property to separate the recoil electrons, which lost energy in the Compton interaction, from the main electron beam.

A magnetic chicane is a series of four dipole magnets, of length d and magnetic field B, placed along the beam line as seen in Figure 2.4. The direction of the magnetic field of the dipoles alternates from one dipole to the next, so that the electrons are eventually bent back to the original beam axis. To avoid causing significant changes to the beam optics, the chicane is designed to be as symmetrical as possible.

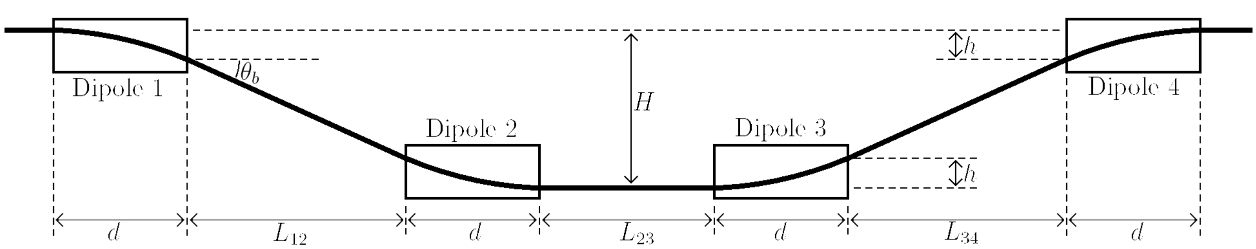

Figure 2.4: **Side view of the magnetic chicane.**

The laser beam is placed such that the laser light overlaps the electron beam between the second and third dipoles. Since the electrons scatter at a small angle with respect to the main electron beam, the recoil electrons continue approximately along the main electron beam line. The recoil electrons, having lost energy in the Compton scattering process, have momenta ranging from the main beam momentum down the Compton edge momentum.

Thus, after the third dipole, the recoil electrons are deflected through a larger angle than the main beam. This is the momentum analyzing of the electrons and results in a spatial separation of the recoil electrons from the main beam. The amount of separation depends on the momentum, or equivalently, the energy lost in the Compton scattering process, (2.2).

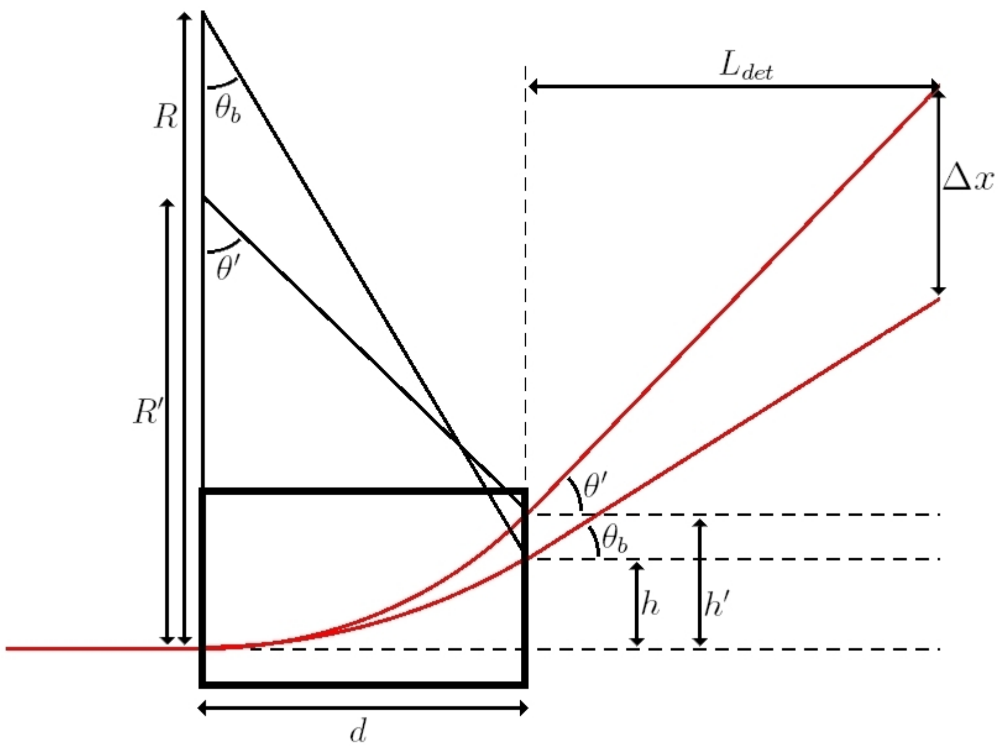

Figure 2.5: **Momentum analyzing the electrons.** Electrons of momentum p and p' get deflected by angles θ_b and θ'.

From Figure 2.5, an electron with momentum p' is deflected by the angle θ' given by

$$\theta' = \sin^{-1}\left(\frac{p}{p'}\sin\theta_b\right) \tag{2.13}$$

after traveling through the same length dipole as an electron with momentum p, bent at an angle θ_b. After exiting the third dipole, the recoil electron is separated from the main beam line by a distance $h' - h$, where $h = R(1 - \cos\theta_b)$, $h' = R'(1 - \cos\theta')$ and R and R' are the radii of curvature of the paths of the undeflected and deflected electrons.

The electrons are spatially separated even more after a free drift distance L_{det} to the electron detector. The final separation of a recoil electron, with momentum p' from the main beam is

$$\Delta x = \frac{p'}{eB}(1 - \cos\theta') - \frac{p}{eB}(1 - \cos\theta_b) + L_{det}(\tan\theta' - \tan\theta_b) \ . \tag{2.14}$$

Referring to Figure 2.4, the proposed chicane design is to use dipole magnets of length $d = 1.0\,\mathrm{m}$. The first and second dipoles, and the third and forth dipoles, would be separated by the same amount, $L_{12} = L_{34} = 2.3\,\mathrm{m}$. The second and third dipoles separated by $L_{23} = 2.0\,\mathrm{m}$ and the chicane will have a maximum vertical beam deflection of $H = 57\,\mathrm{cm}$. This results in a total chicane length of 10.6 m and a beam bend angle of $\theta_b = 10°$ which will require the magnetic field strength in the dipole magnets of $B = 0.675\,\mathrm{T}$.

2.5 Electron and Photon Detection

To map out the Compton asymmetry, either the recoil electrons or the scattered photons must be measured. The magnetic chicane makes it possible to detect both the electrons and the photons without interfering with the electrons in the main beam.

One possible place for an electron detector is after the fourth dipole, which would result in the greatest recoil electron deflection, $\Delta x_1 = 25.7\,\mathrm{mm}$ at the Compton edge. However, in this position, the detector would be subject to synchrotron radiation emitted by the electrons as they are accelerated around the bend in the fourth dipole, (see Section 5.5).

A possibly more desirable position for the electron detector would be 20 cm before the fourth dipole. There is slightly less electron deflection in this position, maximally $\Delta x_2 = 20.3\,\mathrm{mm}$, but there should be significantly less synchrotron radiation to interfere with the detector.

The Compton backscattered photons are scattered at a very small angle, θ_γ, with respect to the beam axis. With the main beam diverted by the third dipole, the photons, whose path is not altered in the magnetic field, continue in a straight line. After the photons exit the third dipole, they can be detected by a photon detector.

This makes it possible to make a measurement of the polarization using the Compton backscattered photons. For the Qweak kinematics, the maximal photon energy is 48.1 MeV. The full energy of the backscattered photons will be detected using a lead-tungstate ($PbWO_4$) fast-scintillating crystal. The photon detector has poorer energy resolution, and must be calibrated using the electron detector.

The rest of this thesis will focus on the recoil electron detector and its design characteristics.

Chapter 3

Electron Detection

To make an accurate extraction of the electron beam polarization, the Compton asymmetry will be mapped out as a function of momentum. The recoil electrons' displacement from the main electron beam, and hence their momenta, will be measured using a *microstrip* detector. This is a device composed of separate readout strips on a piece of semiconducting detector material. The readout strips are arranged horizontally across the detector face such that when an electron travels through the detector, it will hit one of these strips, indicating its vertical displacement from the main beam. The detector's spatial resolution, and thus momentum resolution, depends on the strip pitch, i.e. the center to center distance between adjacent detector elements.

The detector must have a fine strip pitch, a high rate capability, and be resistant to radiation damage, as it will be located as close to the main beam line as possible. The electron detector will be made from diamond semiconductor.

3.1 Diamond as a Semiconductor Detector

Semiconductors are often used in high energy physics experiments in the form of pixel or multistrip detectors because they can have a high spatial resolution and a fast response time.

In a semiconducting material, the passage of ionizing radiation, i.e. high energy electrons, deposits energy in the material. This excites electrons in the valence energy band into the conduction band. This results in a *hole*, in the valence band. The *free* electrons in the conduction band are detached from their parent atoms and are free to move about the crystal. The hole left in the valence band acts a positive charge carrier and is also free to move through the crystal [9].

In a semiconductor detector, Figure 3.1, a potential difference is applied across the semiconductor, creating an electric field across the electrodes. The electron-hole pairs are separated by the field, the electrons drifting to one side of the detector, to the anode, and the holes to the opposite side, the cathode. The electrodes collect the charge, causing a current pulse, which is amplified and analyzed through the electronics.

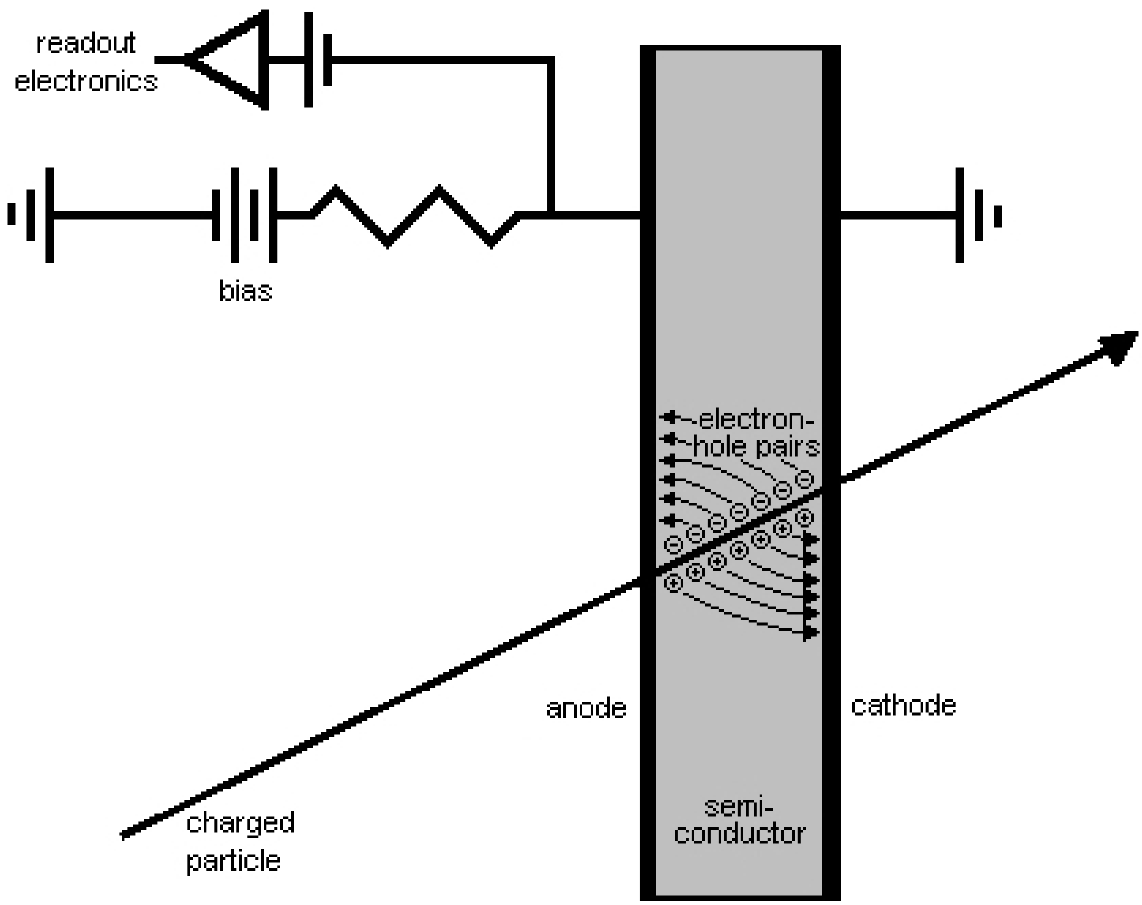

Figure 3.1: **A semiconductor detector**

Possible semiconducting materials that could be used to build the detector include silicon and diamond. Table 3.1 summarizes some of the important characteristics of the two materials.

Diamond has several advantages over silicon. The larger energy gap in the energy band structure of diamond means it is more difficult for electrons to get into the conducting band, meaning that diamond should have less signal noise from thermal excitation. Diamond has a higher rate capability than silicon because it has a faster signal collection. This is because both the electron-hole mobility and the saturation velocity are higher in diamond. Diamond is also more resistant to radiation damage as it takes a higher energy (the displacement energy) to knock an atom out of its place, causing a defect in the structure.

	Silicon	**Diamond**
Band Gap (eV)	1.12	5.49
Dielectric Constant	11.9	5.7
Electron Mobility (cm^2/Vs)	1350	2400
Hole Mobility (cm^2/Vs)	480	2100
Saturation Velocity (cm/s)	0.8×10^7	$1.50/1.05\times10^7$

Table 3.1: **Diamond and silicon semiconductor properties [9, 10]**

However, diamond will yield a smaller signal than silicon. In diamond, it takes more energy to excite an electron into the conduction band, creating an electron-hole pair, thus on average, less electron-hole pairs are created. The charge collection is limited by grain boundaries, impurities, and crystal defects in the synthetic diamond. Because of the quality of the commercially available diamond, the charge collection distance is smaller than in silicon.

3.2 Recoil Electron Detector

Figure 3.2 shows a schematic side view of the Compton electron detector assembly. Four detector planes will be used to ensure efficient detection and to achieve maximum position resolution. To protect the detector from damaging radiation, the detector will be equipped with a motion mechanism that will move the detector away from the electron beam when not in use.

The detector will be located in an enlarged section of the beam pipe, while the motion mechanism and readout electronics will be outside of the pipe.

The electron detector will be made out of large-area-polycrystalline diamond grown via chemical vapour deposition. Each plane will be fabricated from planar diamond, 2.1 cm $\times$ 2.1 cm $\times$ 300 μm. The two faces must first be metallized with a Ti/Au or Cr/Au layer to form the electrodes. The readout strips will then be etched into one face by photolithography and chemical etching. The detector will be attached to a carrier board, and the detector strips wirebonded to strips on the carrier board. The detector will be readout using standard semiconductor electronics.

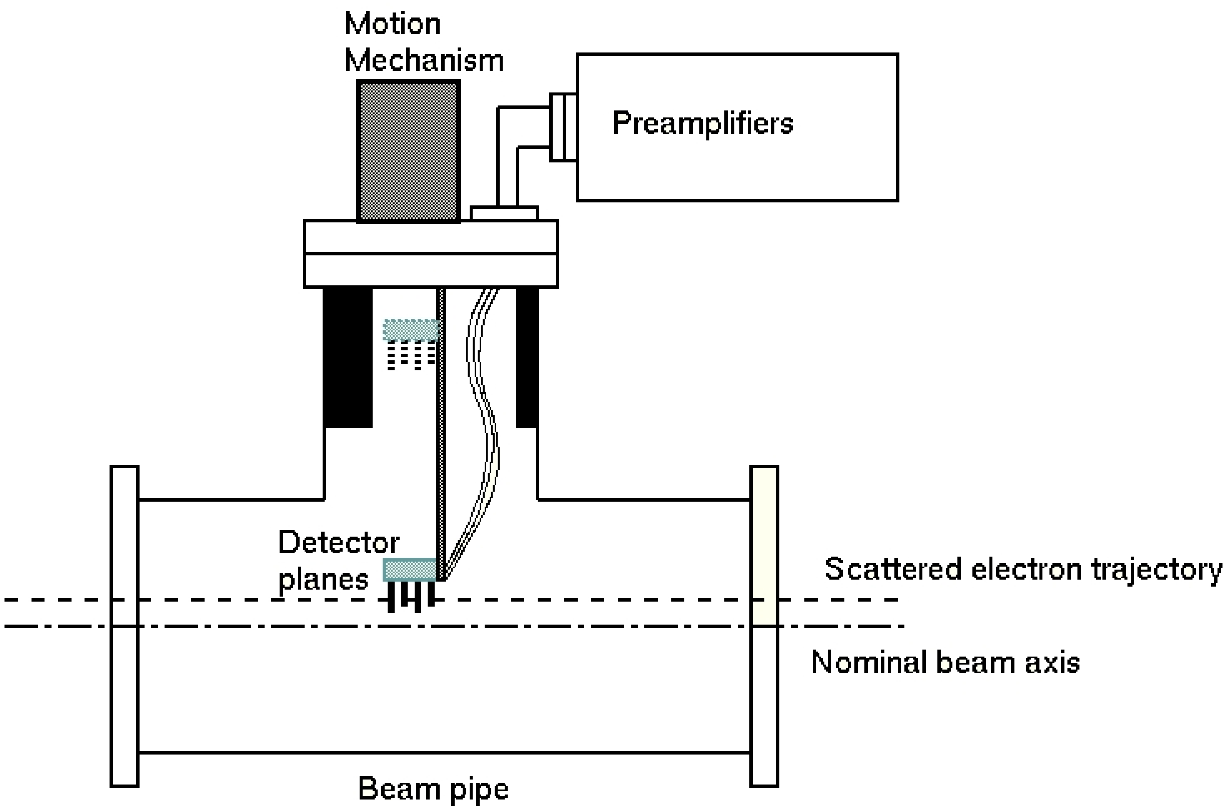

Figure 3.2: **Electron detector and motion mechanism.**

Chapter 4

Compton Polarimeter Simulation

4.1 GEANT Simulation

To optimize the design and quantify systematic uncertainties of the proposed electron detector, a simulation of the magnetic chicane, Compton interaction, and electron deflection and detection was used [11]. The simulation was written in FORTRAN, using GEANT version 3 [12]. GEANT stands for GEometry ANd Tracking.

GEANT is a simulation tool used to design and optimize detectors, develop and test analysis programs, and help interpret experimental results from high energy physics experiments. GEANT uses a library of physics processes to track particles through a simulated environment and measure how they interact with the environment and detectors.

Geant simulates interactions such as Compton scattering, the photoelectric effect, pair production, bremsstrahlung, and synchrotron radiation. Geant also calculates how particles interact with fundamental fields such as electric and magnetic fields.

The GEANT simulation allows us to describe the experimental setup of the Compton Polarimeter using a structure of geometrical volumes. Figure 4.1 shows the geometry used in the simulation. Visible is the magnetic chicane, with the beam line coming in from the left of the image, beam pipes, and the electron and photon detectors.

The magnetic dipoles are regions defined to have a magnetic field within them. While an electron is tracked through the magnetic field region, GEANT calculates the force on the electron and alters the trajectory to account for this. The beam pipes are evacuated tubes that the electrons travel though between the dipoles, and the detectors are volumes filled with a sensitive material.

The simulation uses event generators to create particles and then tracks these particles

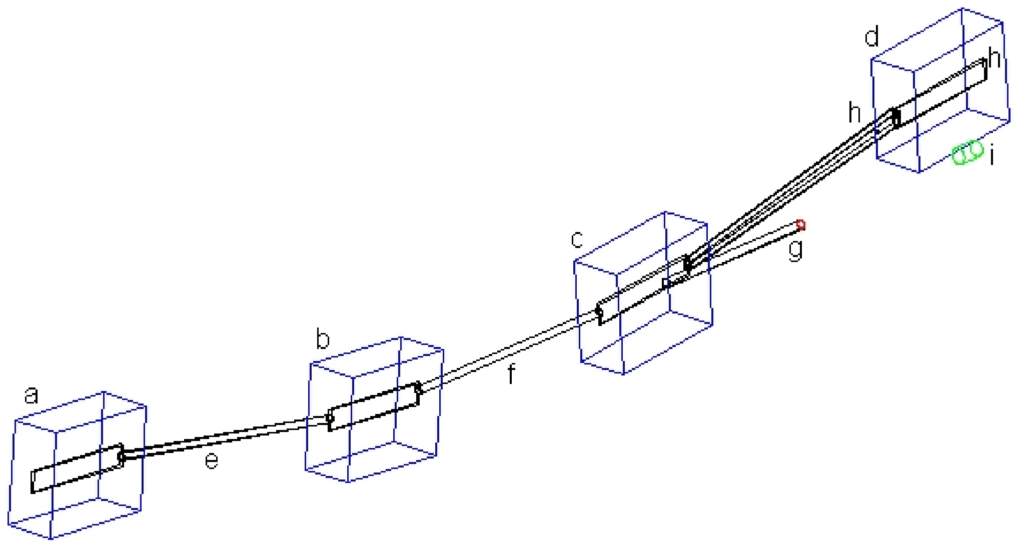

Figure 4.1: **Magnetic chicane geometry in GEANT simulation.** (a-d) magnetic dipoles, (e) beam pipe, (f) Compton interaction region, (g) scattered photon exit port, (h) electron detector positions, (i) photon detector.

through the simulated environment. The simulation records the response of the detectors, properties of the Compton electrons and photons, and properties of the Compton interaction such as the cross-section and the asymmetry. GEANT also makes it possible to visualize the environment and trajectories of the particles.

4.2 Event Generators

Included in the simulation are several different *event generators*, used to perform the various studies. The main generator is the Compton generator, in which an event is created in the region between the second and third dipoles. Figure 4.2 shows a single Compton event.

An electron and its backscattered photon are created at the point where the laser beam crosses the electron beam using Monte Carlo techniques. The cross section and asymmetry are calculated at the fractional energy, ρ, of the backscattered photon. The electron is tracked through the magnetic chicane and hits the electron detector. The photon travels out the photon exit port and interacts with the photon detector.

The synchrotron generator creates electrons at the entrance to the magnetic chicane and

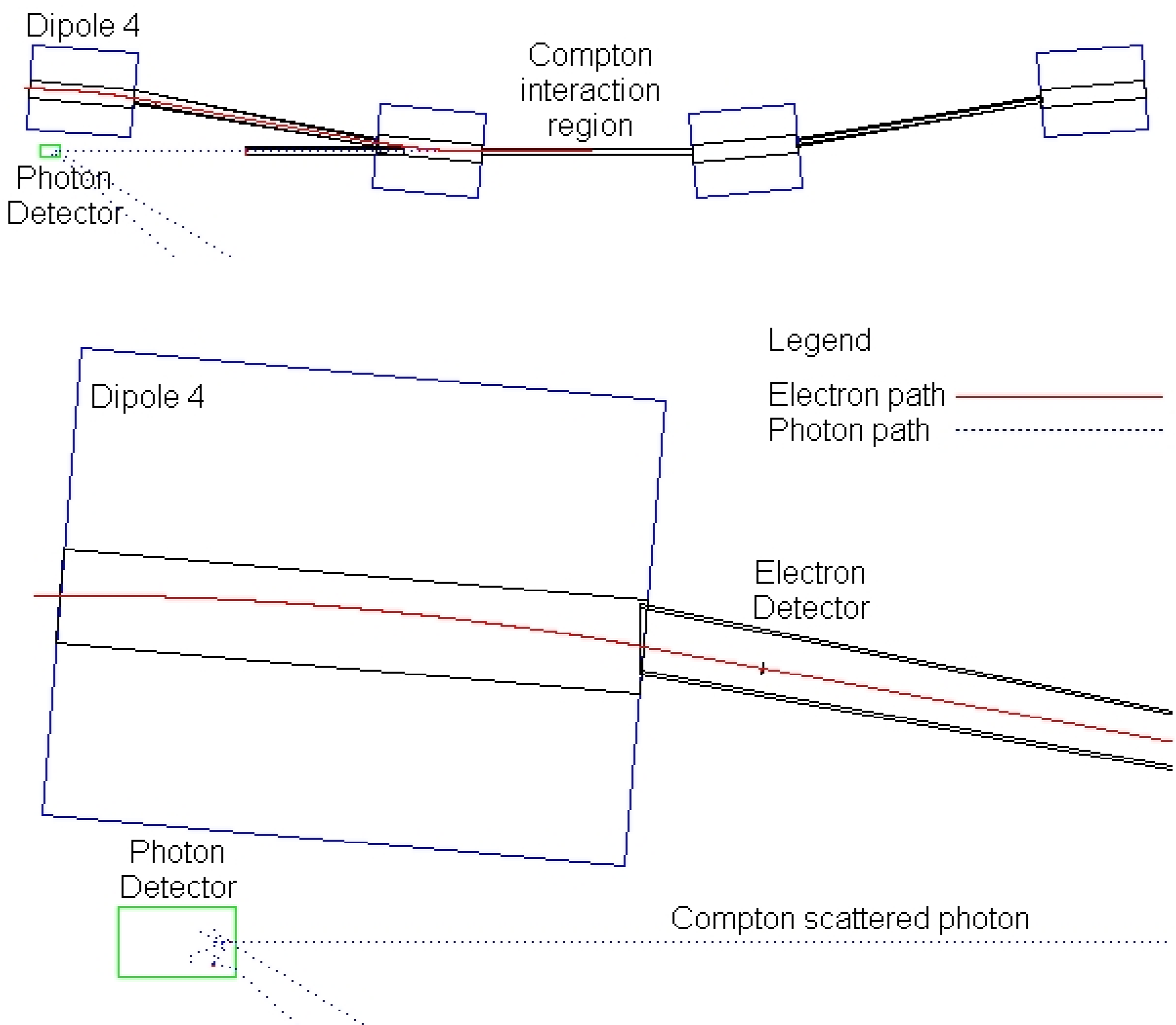

Figure 4.2: **A Compton event.**

tracks it through the chicane. GEANT computes the energy lost by synchrotron radiation during each step and generates a synchrotron photon from this. The photon is emitted tangent to the path of the electron and is tracked through the simulation volume.

There are other event generators included in the simulation that have not been used in the current studies. These include a bremsstrahlung generator, which fills the beam pipes with a residual gas and is used to study the interactions between the electrons in the beam and the gas, and a beam halo generator which adds *tails* to the main beam envelope.

Using this simulation, studies can be performed on the design of the electron detector for the Compton polarimeter such as:

- the effect of strip pitch on polarization measurement,
- how different polarization extraction methods differ,
- how the detector's position in the chicane affects background rates.

Chapter 5

Results

5.1 Electron Detector Strip Map

For each generated Compton interaction, GEANT calculates two weighting factors from the energy of the scattered photon, ρ: the theoretical asymmetry, A_i, and cross-section, σ_i. GEANT saves these values in a data structure for each event. Other parameters are saved in this data structure such as the strips hit in the electron detector and how much energy was deposited in each strip, and the detected energy of the backscattered photon.

After generating a significant number of events, these results, saved by GEANT, can be used to form a *strip map* of the number of hits in each strip of the electron detector, i.e. the number of Compton electrons created at different energies. As can be seen on the plot, Figure 5.1a, the number of hits in each strip is approximately constant over all strips up to the Compton edge. This is because in the simulation, the Compton events are generated *flat* in photon energy, ρ, that is they are chosen randomly between $\rho = 0$ and $\rho = 1$.

A more realistic distribution of Compton electrons can be created using the cross section, σ_i, as the event weight. The strip map formed in this manner is more like what would be seen in the actual physical electron detector, Figure 5.1b.

5.2 Asymmetry

The polarization is measured from the experimental asymmetry measured in the electron detector, A_{exp}, by measuring n^+ and n^-. The experimental asymmetry is defined as

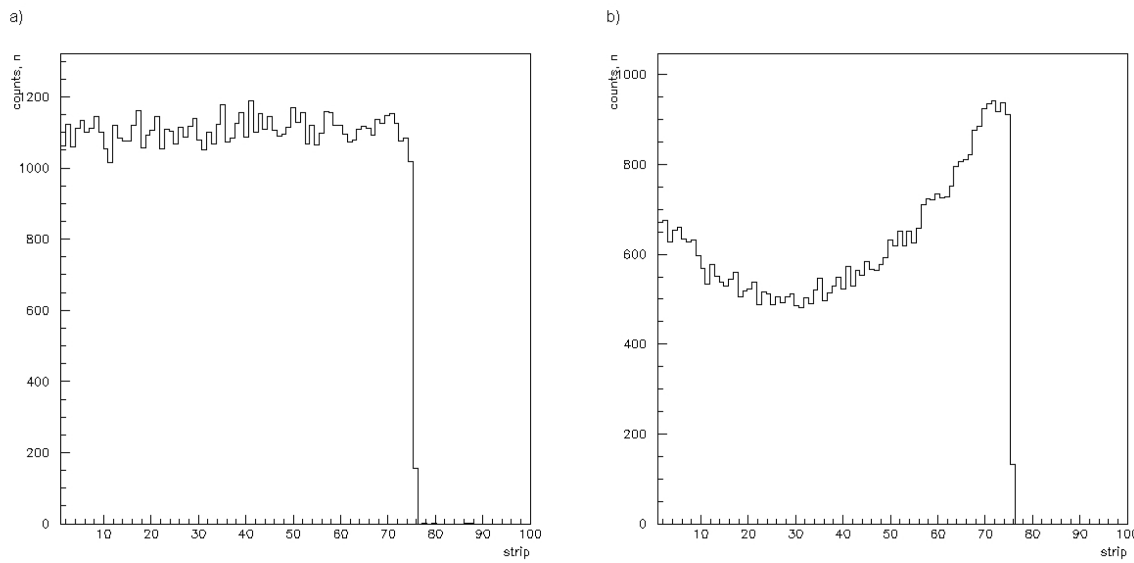

Figure 5.1: **a) Unweighted strip map, b) Cross section weighted strip map**

$$A_{exp} = \frac{n^+ - n^-}{n^+ + n^-} = \frac{\sigma^+ - \sigma^-}{\sigma^+ + \sigma^-} \tag{5.1}$$

where σ^+ and σ^- are the spin dependent differential cross sections. The simulation does not create n^+ or n^- events, but as mentioned earlier, the simulation calculates the asymmetry and unpolarized cross sections for each event. The spin dependent cross sections can be calculated from these two weighting factors by $\sigma_i^+ = \frac{1}{2}(\sigma_i + A_i\sigma_i)$ and $\sigma_i^- = \frac{1}{2}(\sigma_i - A_i\sigma_i)$, giving

$$(\sigma^+ - \sigma^-)_i = A_i\sigma_i \quad \text{and} \quad (\sigma^+ + \sigma^-)_i = \sigma_i \ . \tag{5.2}$$

So, by summing over all the events striking a single strip, the average asymmetry for that strip is,

$$A_{exp} = \frac{\sum\limits_i A_i\sigma_i}{\sum\limits_i \sigma_i} \ . \tag{5.3}$$

By this operation, the simulated asymmetry measured in the electron detector can be calculated for each strip, as plotted in Figure 5.2. Also shown on the plot is the theoretical asymmetry, A_ℓ, as the dotted line.

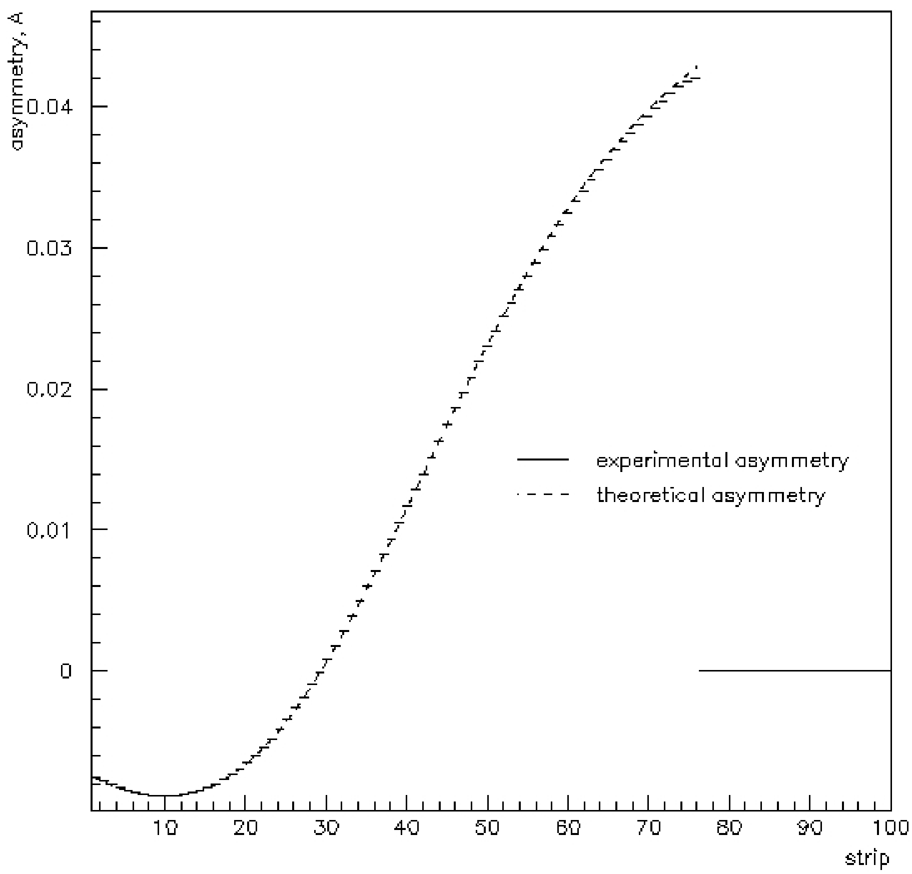

Figure 5.2: **Simulated Compton asymmetry measured in electron detector with 210 μm strip pitch**

5.3 Polarization Determination Methodology

The polarization of the electron beam will be measured using equation (2.11), that is $P_e = \frac{A_{exp}}{P_\gamma A_\ell}$. In the simulation the laser beam is circularly polarized with $P_\gamma = 1$. The electron beam polarization is then $P_e = \frac{A_{exp}}{A_\ell}$. The extracted polarization is expected to agree with unity. Disagreement would be an idication of systematic effects.

Curve Fitting Method

There are several methods of measuring the ratio $\frac{A_{exp}}{A_\ell}$. One method is to fit the asymmetry function, equation (2.9), to the experimental asymmetry. This fit involves three curve parameters: P_1, the vertical stretch factor, P_2, the horizontal offset of the detector, and P_3, the horizontal stretch factor. The fitting function, as a function of strip x, is

$$A_{exp} = P_1 \frac{(1-((x-P_2)P_3)(1+a))\left(1-\frac{1}{(1-((x-P_2)P_3)(1-a))^2}\right)}{\left[\frac{((x-P_2)P_3)^2(1-a)^2}{1-((x-P_2)P_3)(1-a)} + 1 + \left(\frac{1-((x-P_2)P_3)(1+a)}{1-((x-P_2)P_3)(1-a)}\right)^2\right]} \ . \tag{5.4}$$

Using this method, the ratio, $\frac{A_{exp}}{A_\ell}$, is taken as vertical stretch factor, $\frac{A_{exp}}{A_\ell} = P_1$. This method for extracting the polarization has a small intrinsic error associated with it. It assumes that the horizontal fit parameters give a perfect fit to the theoretical asymmetry, and the vertical scale includes all the polarization information. However, it is also possible for the horizontal fit parameters to affect the polarization, but this method does not take this into account.

Integral Method

A second method, which will likely be the method used for the Qweak Compton polarimeter, is to integrate under the experimental asymmetry curve from the asymmetry zero crossing to the Compton edge. The integral of the experimental asymmetry is done by doing a weighted sum over all events past the asymmetry zero

$$\langle A_{exp} \rangle = \frac{\sum\limits_i A_i \sigma_i}{\sum\limits_i \sigma_i} \ . \tag{5.5}$$

And the theoretical integration can be done using numerical integration techniques,

$$\langle A_\ell \rangle = \frac{\int_{\rho_0}^{\rho_{max}} d\rho \frac{d\sigma}{d\rho} A(\rho)}{\int_{\rho_0}^{\rho_{max}} d\rho \frac{d\sigma}{d\rho}} \ , \tag{5.6}$$

where ρ_0 is the scattered photon energy at the asymmetry zero and ρ_{max} is the Compton edge. Thus, using the integration method the ratio is $\frac{A_{exp}}{A_\ell} = \frac{\langle A_{exp} \rangle}{\langle A_\ell \rangle}$.

It was found that for this application, the integration method was very sensitive to the location of the asymmetry zero. For a strip pitch of 210 μm, the extracted polarization varied by approximately 2% if the asymmetry zero was off by only a single channel. If the detector was moved slightly, causing the asymmetry zero to lie in a new strip, the polarization measurement also changed.

For these reasons, it was determined that the curve fitting method for extracting the polarization would be the best method to use in this analysis. The curve fitting method was used in the subsequent studies.

5.4 Strip Pitch Design Study

The strip pitch of the electron detector is the center to center distance between two adjacent detector elements. When a scattered electron passes through the detector, it strikes one of the strips depending on the electron's momentum. To form the asymmetry curve, the momentum of the scattered electron must be known as accurately as possible. The locations of the Compton edge and asymmetry zero are used to calibrate the detector. Thus, the accuracy of the momentum measurement is directly related to the strip pitch.

Ideally the strip pitch would be as fine as possible. If the strip pitch were infinitely small, the momentum of the scattered electrons can be determined exactly, which should theoretically lead to a perfect measurement of the polarization. In reality, the strip pitch must be finite. The main constraint on the strip pitch is from fabrication and electronics costs.

To determine how the polarization measurement varies with strip pitch, the simulation can be run with different detector strip pitches. Figure 5.3 shows the resulting experimental asymmetry curves generated from 10,000 events with three different strip pitches, 105 μm, 1050 μm, and 2100 μm.

To quantify the dependence of the polarization on the strip pitch of the detector, the polarization is determined for different strip pitches. Using the curve fitting method for determining the polarization, Table 5.1 lists the measured polarizations and Figure 5.4 is

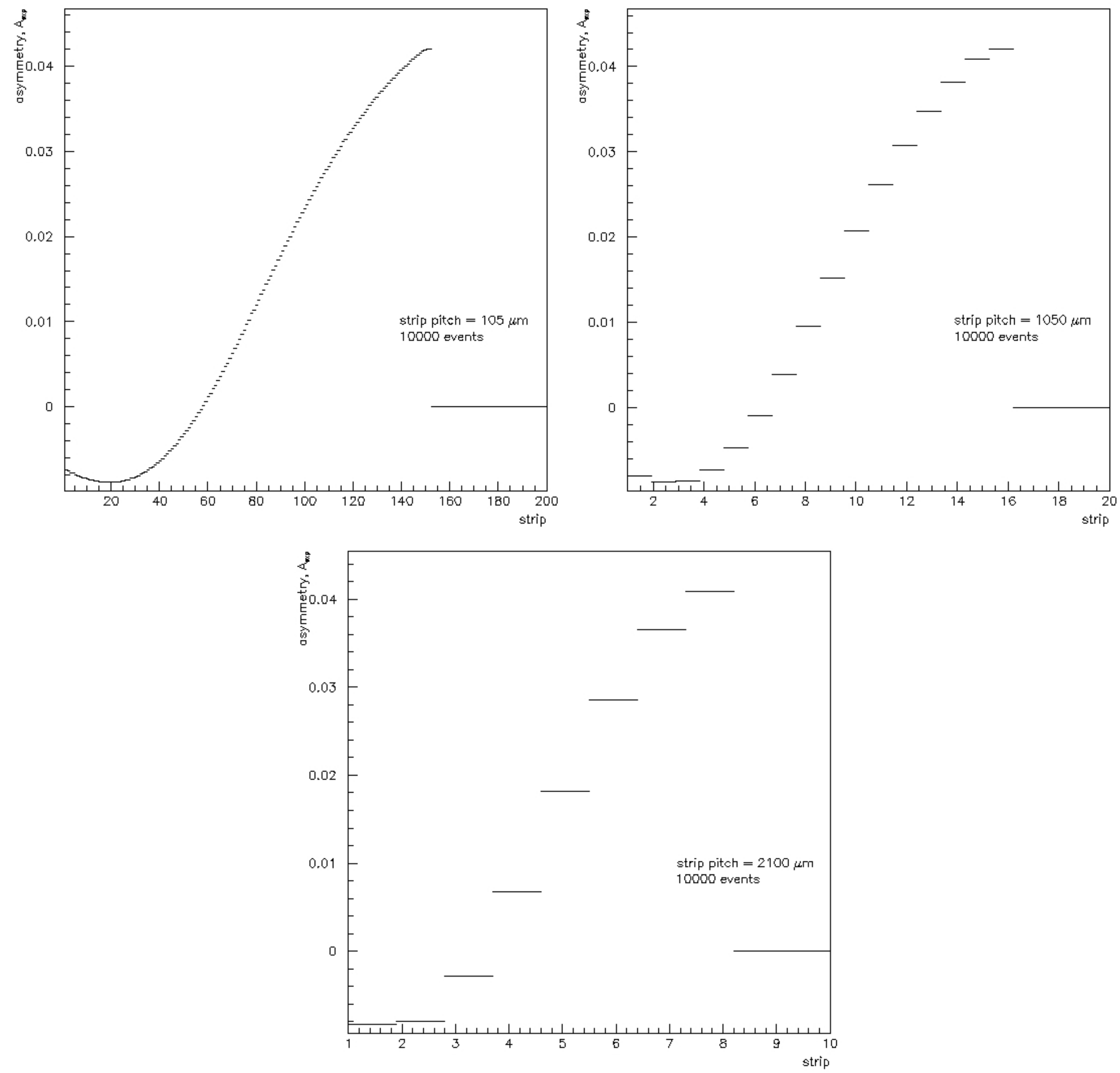

Figure 5.3: **Simulated experimental asymmetry with different strip pitches**

plot of how the error in polarization, δP, varies with strip pitch.

Strip Pitch (μm)	**Polarization**	$\delta P/P$ (%)	**Strip Pitch (μm)**	**Polarization**	$\delta P/P$ (%)
50	.9902	0.98	840	.9847	1.53
105	.9899	1.01	1050	.9873	1.27
210	.9905	1.06	1500	.9856	1.44
300	.9884	1.16	1750	.9823	1.77
420	.9885	1.15	2100	.9816	1.84
600	.9854	1.45	2400	9800	2.00

Table 5.1: **Polarization measurements with different strip pitches.** Polarization extracted using curve fitting method.

As can be seen on the plot, the error in the polarization depends linearly on strip pitch. By fitting a straight line to the curve, it was found that

$$\frac{\delta P}{P} = 0.0807 \frac{\Delta x}{x_{max}} + 1.01 \ , \tag{5.7}$$

where Δx is the strip pitch and x_{max} is the scattered electron to beam separation at the Compton edge. As the strip pitch approaches zero, the calculated relative error does not approach zero, but has a minimum value of 1.01%. The reason for this is likely the fact that the electron beam has a finite width that is of the order of the strip pitch. It could also be due to an intrinsic error related to the polarization extraction method or from effects of the detector.

The uncertainty, $\delta P/P$ in equation (5.7), depends not only on the strip pitch, but also on the amount of deflection of the electrons relative to the strip pitch. An increased deflection at the Compton edge, x_{max}, would result in a more accurate measurement of the individual electron's momentum, and thus a more accurate extraction of the polarization.

A greater electron deflection can be achieved by using a larger chicane bend angle or by placing the electron detector further down the chicane, i.e. after the fourth dipole rather than before. After the dipole, the maximum deflection would be $\Delta x_1 = 25.7\,\text{mm}$, whereas 20 cm before the dipole, the maximum deflection would be $\Delta x_2 = 20.3\,\text{mm}$.

Nonetheless, the current studies indicate that the proposed strip pitch of 210 μm should be sufficient to acquire the polarization of the electron beam to 1%.

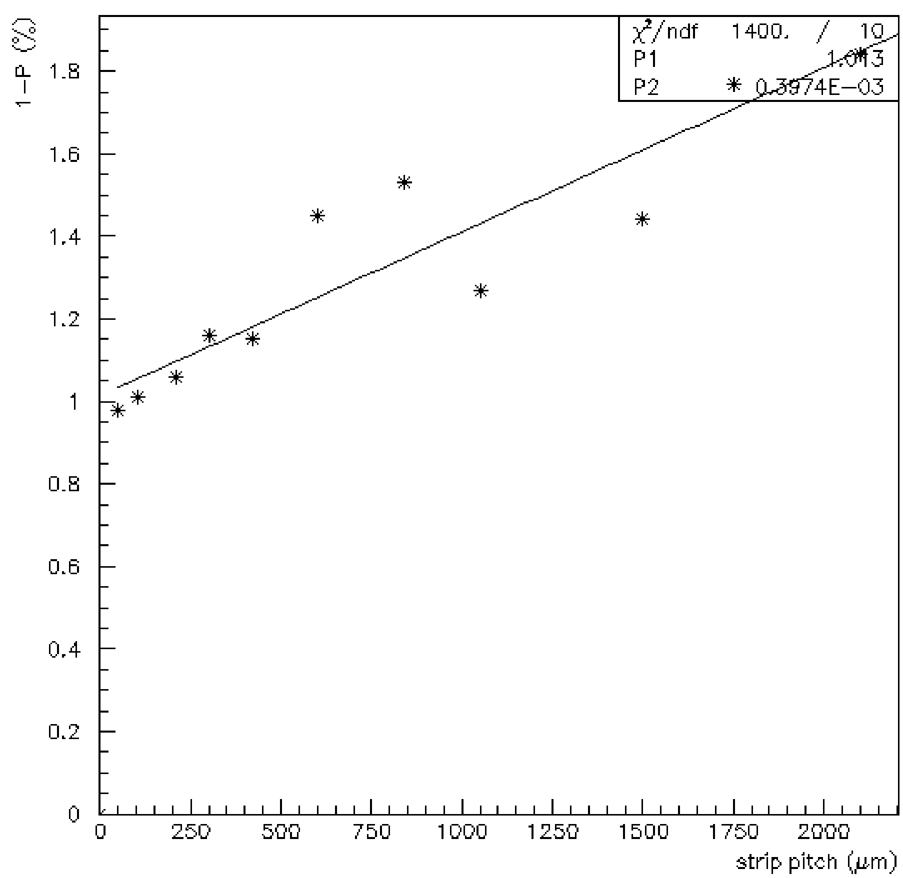

Figure 5.4: **Error in polarization at different strip pitches**

5.5 Synchrotron Radiation

Another study performed using the GEANT simulation is a visual study of the effect of synchrotron radiation. When the electrons travel through the dipole magnets, they are accelerated and emit radiation. This radiation is called synchrotron radiation and can cause significant problems with the operation of the Compton polarimeter if it strikes either the electron or photon detectors.

For relativistic electrons, synchrotron radiation is emitted nearly tangent to the electrons path as it travels through the dipole magnets. Thus, positions after the dipoles are directly in line with the radiation. Figure 5.5 is a picture generated by the simulation showing where the synchrotron radiation is emitted and what areas are in line with this radiation. The region directly behind the fourth dipole is enlarged to show the details.

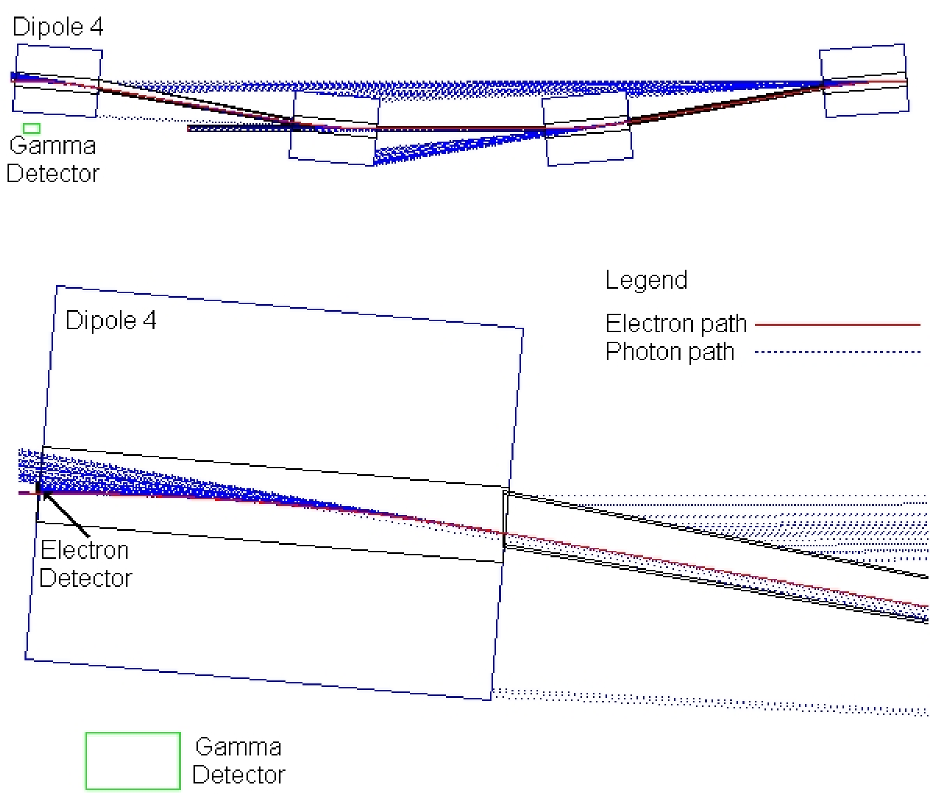

Figure 5.5: **Synchrotron radiation emitted by the electron beam**

With the detector placed in the position behind dipole four, 5 mm from the electron beam, after 100,000 events, 82,318 photons, with energy over 10.0 keV, hit the detector. With the detector located before the fourth dipole, after running 12,000,000 events, only 3 photons hit the detector. The background due to photons above 10 keV would be expected to be smaller by a factor of 3×10^6 before the fourth dipole versus after.

The photons striking the detector when the detector is in front of the fourth dipole are due to synchrotron photons bouncing off the inner surface of the beam pipe. However, the simulation does not properly take the beam pipe reflectivity into account so this result is only a first estimate.

As expected, the area directly behind dipole four is directly in line with the radiation emitted by the electrons as they travel through the dipole, whereas the region before the fourth dipole has significantly less synchrotron radiation.

Chapter 6

Conclusion

The theory behind the Qweak Compton polarimeter has been discussed and the proposed experimental device presented. The GEANT simulation was used to perform design studies on the electron detector. Using the method of fitting the theoretical asymmetry function to the experimentally acquired asymmetry to extract the polarization, several conclusions can be made from the simulation studies. It was found that the proposed electron detector strip pitch of 210 μm should be sufficient to make a measurement of the electron beam polarization to an accuracy of 1%.

A study on the location of the electron detector was also performed and it was found that background rate caused by synchrotron radiation was much higher in the position after the fourth dipole versus before the dipole.

There are several improvements that could be made to the simulation. The simulation code could be modified to correctly simulate the reflectivity of the beam pipe. This could result in a more realistic study of background rates. Improvements could also be made to the polarization extraction method, possibly by fitting both the asymmetry and the cross section simultaneously.

Bibliography

[1] D. Griffiths, *Introduction to Elementary Particles*, WILEY-VCH Verlag GmbH & Co. KGaA, Weinheim (2004).

[2] J. Erler *et al*, "The Weak Charge of the Proton and New Physics", hep-ph/0302149 (2003).

[3] S. Willocq, " Physics at the Z-Pole with SLD", SLAC-R-508 (1996)

[4] A. Deandrea, "Atomic Parity Violation in Cesium and Implications for New Physics", Phys. Lett. B **409**, 227 (1997).

[5] P.L. Anthony *et al* (SLAC E158 Collaboration), "Precision Measurement of the Weak Mixing Angle in Møller Scattering" Phys. Rev. Lett. **92**, 181602 (2004).

[6] G.P. Zeller *et al* (NuTeV Collaboration), "A Precise Determination of Electroweak Parameters in Neutrino-Nucleon Scattering", Phys. Rev. Lett. **88**, 091802 (2002).

[7] Qweak website, `http://www.jlab.org/qweak/`, (2006).

[8] G. Bardin *et al*, "Conceptual Design Report of a Compton Polarimeter for Cebaf Hall A" (1996).

[9] W.R. Leo, *Techniques for Nuclear and Particle Physics Experiments*, Springer-Verlag, Berlin (1994).

[10] M. Prelas *et al*, *Handbook of Industrial Diamonds and Diamond Films*, Marcel Dekker Inc., New York (1998).

[11] R. Jones, Compton Polarimeter Simulation, `http://zeus.phys.uconn.edu/qweak/compton_geant/`, (2003).

[12] CERN Application Software Group and Computing and Networks Division, "GEANT Detector Desciption and Simulation Tool", CERN (1994).